applied sciences

MDPI

Article

Facile Fabrication of 3D Hierarchically Porous Carbon Foam as Supercapacitor Electrode Material

Yunfang Gao *, Liangpo Cai, Xin Xu and Jie Ying

State Key Laboratory Breeding Base of Green Chemistry-Synthesis Technology, College of Chemical Engineering, Zhejiang University of Technology, Hangzhou 310014, Zhejiang, China; lpcai@zjut.edu.cn (L.C.); x_xin2008@163.com (X.X.); zizitong@163.com (J.Y.)

* Correspondence: gaoyf@zjut.edu.cn; Tel.: +86-571-8832-0306

Received: 7 March 2018; Accepted: 2 April 2018; Published: 5 April 2018

Abstract: A hierarchically porous 3D starch-derived carbon foam (SCF) with a high specific surface area (up to 1693 $m^2 \cdot g^{-1}$) was first prepared by a facile solvothermal treatment, in which Na_2CO_3 is used as both the template and activating agent. The hierarchically porous structure and high specific area endow the SCF with favorable electrochemical properties such as a high specific capacitance of 179.6 $F \cdot g^{-1}$ at 0.5 $A \cdot g^{-1}$ and a great rate capability and cycling stability, which suggest that the material can be a promising candidate for energy storage applications.

Keywords: starch; carbon foam; Na_2CO_3 self-sacrificing template; hierarchically porous; supercapacitor

1. Introduction

With the continually increasing demand for energy and the limited availability off ossil fuels, it is imperative to urgently develop advanced electrochemical devices with high efficiency, renewability, and low price [1,2]. Supercapacitors based upon electrical double-layer capacitance have played a vital role in energy storage devices owing to their distinct merits, including rapid charge/discharge rate, superior power density, and extremely long cycle stability [3]. Various carbonaceous materials are employed in electrical double layer capacitors such as activated carbon, carbon nanotubes, and graphene because of their robust porosity, high electrical conductivity, and stable physicochemical properties [4,5]. However, conventional carbon-based electrical double layer capacitors suffer from a low specific capacitance and poor rate capability because of diffusion restriction between internal pores and electrolyte ions at high rate conditions [6].

Recently, 3D hierarchical carbonaceous materials with high surface areas and special porous structures have attracted considerable interests for their high performance on supercapacitors [7,8]. The hierarchically porous structure that couples various pores provides highly efficient ion transport channels through the mesopores/macropores and high capacitance from the micropores/mesopores [9]. Li et al. used KOH and resol to synthesize 3D hierarchical porous carbon with a high specific surface area. The obtained material shows excellent supercapacitive performances in a 6 M KOH electrolyte [10]. However, the most common activating agents (KOH and NaOH) are highly corrosive [11], which may damage the equipment and hamper the industrial production. Herein, we utilize weakly corrosive Na_2CO_3 for activation to prepare 3D hierarchically porous starch-derived carbon foam (SCF), which plays the role of the template of macropores as well. Meanwhile, starch is a kind of cheap and available carbon source. Therefore, this facile pathway makes carbon foam for supercapacitors easier to produce in high volumes.

2. Experimental

Starch was utilized as the carbon source through a facile solvothermal process. Typically, Starch and Na_2CO_3 were mixed with a mass ratio of 1:1 in 75 mL ethyl alcohol. Afterward, the mixture was

transferred into a 100 mL Teflon-lined stainless steel autoclave, solvothermally treated at 180 °C for 16 h, and then naturally cooled down to ambient temperature. The product was filtered and dried in a vacuum at 80 °C for 24 h. The sample was heated from an ambient temperature to 850 °C at the rate of 5 °C/min in a nitrogen atmosphere and held at 850 °C for 1.5 h. Finally, the resulting product was washed with a dilute HCl solution to get rid of the residual Na_2CO_3 and deionized the water to a neutral pH, and dried at 80 °C for 24 h in a vacuum oven. The obtained sample was denoted as SCF. For comparison, the pure starch without Na_2CO_3 was dealt with otherwise similar conditions, the product was denoted as SC.

The morphologies of the samples were characterized using a scanning electron microscope (SEM, Hitachi S4800, Tokyo, Japan). The X-ray diffraction (XRD) patterns were recorded with an X-ray diffractometer (PANalytical, Almelo, The Netherlands) with Cu Kα radiation (λ = 0.1542 nm). The Raman spectra were measured on a Micro Raman Spectrometer (JOBIN YVON, Paris, France) with an excitation wavelength of 632.8 nm. The specific surface area and analysis of porosity for materials were characterized by N_2 adsorption/desorption isotherms at 77 K with an ASAP 2010 instrument (Micromeritics, Norcross, GA, USA). The specific surface area and pore size distribution were determined according to the Brunauer–Emmett–Teller (BET) equation and the non-local density functional theory (NLDFT), respectively. The microspore volume (Vmic) was analyzed by the t-plot method. Microporosity was the ratio of micropore volume to total volume.

All electrochemical measurements were performed in a three-electrode setup: a titanium plate coated with slurry as the working electrode, a platinum foil as the counter electrode, and a saturated mercurous sulfate electrode (MSE) as the reference electrode. A solution containing 5 M H_2SO_4 served as the electrolyte at room temperature. Cyclic voltammograms (CV) and galvanostatic charge/discharge (GCD) were measured by an electrochemical workstation (CHI 660D). The working electrodes were prepared with the as-prepared materials, acetylene black, and PVDF (Polyvinylidene Fluoride) in a mass ratio of 8:1:1. The resulting slurry was dropped evenly onto the titanium sheet substrate (1 cm × 1 cm) and dried at 70 °C in a vacuum oven overnight. The loading weight was controlled to be 1 ± 0.1 mg. Then the dried finished electrode was immersed in an H_2SO_4 (5 M) solution for infiltrating the active compositions completely. Electrochemical impedance spectroscopy (EIS, Nyquist plots) was carried out in the three-electrode system at an open circuit potential over a frequency range from 0.01 Hz to 100 kHz with a 10 mV amplitude.

The capacitance values were calculated from cyclic voltammetry curves according to the following formula:

$$C = \frac{\int_{V_a}^{V_c} I(V)dV}{2 \times m \times v \times (V_c - V_a)}, \quad (1)$$

where C is the specific capacitance, I is the current value of the CV curve, v is the scanning speed of the CV curve, m is the mass of the active material, and (Vc–Va) is the potential window.

The capacitance values were also calculated from galvanostatic charge-discharge curves according to the following formula:

$$C = \frac{I \times dt}{m \times (V_c - V_a)}, \quad (2)$$

where C is the specific capacitance, I is the current value of the GCD curves, dt is the time of the galvanostatic discharging, m is the mass of active material, and (Vc–Va) is the potential window.

3. Results

Compared to the smooth surface of starch-derived carbon (SC) in Figure 1a, there are plenty of macroscopic pores evenly embedded in the carbon matrix of SCF (Figure 1b). The higher magnification SEM images of SCF (Figure 1c,d) display a 3D structure with macroporesthe size of 100–500 nm are interconnected to others by smaller pores. It evidently shows that Na_2CO_3 induces the formation of hierarchically porous texture. Figure 2 shows the synthesis steps and presumable mechanism

for starch-derived carbon foam. Na_2CO_3 can act as the template to produce macropores due to the insolubility in ethanol system and the drastic solvothermal treatment promotes uniform mixing of sodium carbonate with starch. Moreover, the Na_2CO_3 template decomposes and releases CO_2 that comes from inside the starch-derived carbon matrix serving as an activating agent to activate the carbon material producing micropores and mesopores as well as the enlarging pore sizes. This effect was named as the "CO_2 inner-activation effect" [12], which can beconfirmed by the Nitrogen adsorption-desorption results. Additionally, macroporesand large mesoporescan serve on ion-buffering reservoirs and increase the accessibility of the smaller pores [13], in terms of improving the rate performance.

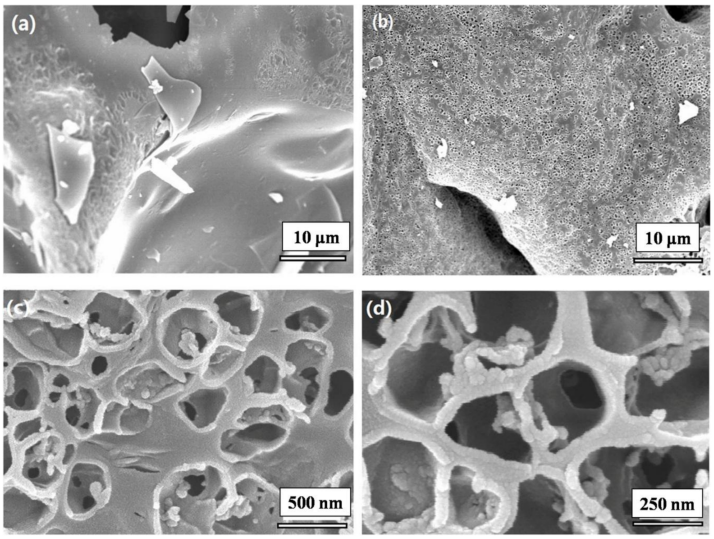

Figure 1. (**a**) The scanning electron microscope (SEM) image of starch-derived carbon; (**b**)–(**d**) various magnification SEM images of starch-derived carbon foam SCF.

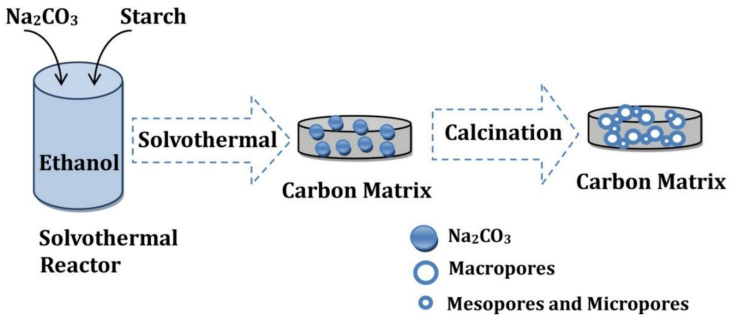

Figure 2. The synthesis steps and presumable mechanism for starch-derived carbon foam.

To further determine the porous structure of SCF, Nitrogen (77 K) adsorption-desorption is performed, showing that the BET specific surface area and pore volume of SCF reaches 1693 $m^2 \cdot g^{-1}$ and 1.106 $cm^3 \cdot g^{-1}$, respectively. The micropore volume of SCF calculated by thet-plot method is 0.255 $cm^3 \cdot g^{-1}$ and the corresponding microporosity is 23%. Figure 3a confirms that the as-prepared sample exhibits a mixture of Type I and IV isotherm with an H4-typehysteresis loop in the relative pressure range of 0.4–1.0 [14], demonstrating that not only do abundant micropores exist in this material, but ample mesopores exist as well [15]. In comparison, SC shows Type IV isotherm and the nitrogen adsorption capacity is relatively smaller (Figure S1) [16]. In Figure 3a, the strong steep adsorption uptake at a low relative pressure indicates a considerable number of micropores [17]. The adsorption plateau at a high relative pressure is not observed, implying the existence of

macropores [9] which consist with the result of SEM images. In addition, pore size distribution calculated with non-local density functional theory NLDFT theory can be noted in Figure 3b. Plentiful peaks at tens of a nanometer testify the large mesopores. As is shown in the inset of Figure 3b, sharp peaks with pore sizes less than 2 nm and between 2 to 6 nm suggest the existence of micropores and small mesopores. Herein, the 3D structure of SCF in which macroporesare interconnected by extensive micropores and mesopores, which is favorable to the electrochemical performance [18], is verified.

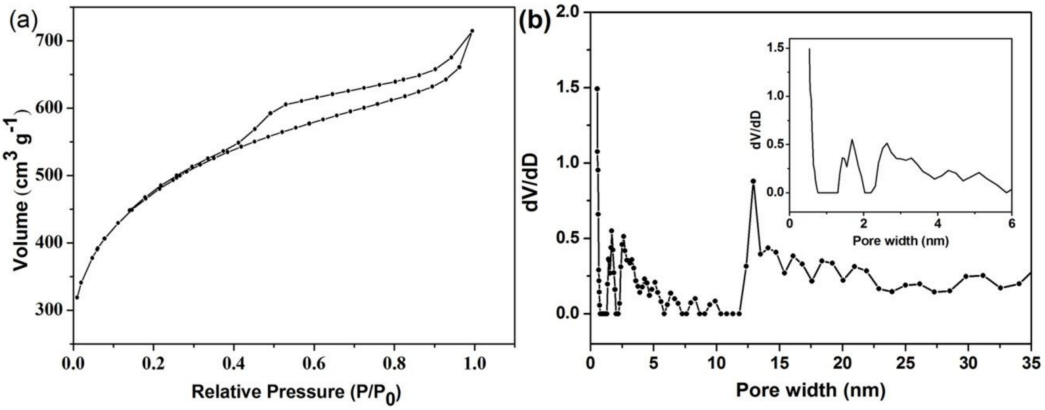

Figure 3. (**a**) The N_2 adsorption/desorption isotherm of SCF and (**b**) the corresponding pore size distribution calculated by the non-local density functional theory NLDFT model with the enlarged image in the inset.

The XRD patterns (Figure 4) of as-prepared samples exhibit two broad peaks at 2θ values of 22.5° and 43°, which can be attributed to the amorphous characteristics of SCF and SC [19]. These broad peaks manifest that no evident graphitization happened during the formation. Obviously, the peaks of SCF are weaker and broader than what SC shows. It indicates the more disordered structure, which is further confirmed by the Raman spectra where the D band (1335 cm^{-1}) of carbon is caused by the disorder groups and defects, while the G band at 1588 cm^{-1} is on behalf of sp^2 domains and the 2D band (~2700 cm^{-1}) manifests the graphitic degree [20]. It is well known that the lower the I_D/I_G ratio, the higher the graphitization degree. The I_D/I_G of SCF is 1.16 higher than SC (0.98), showing the strengthened intensity of the disorder and defects induced by the Na_2CO_3 activation [21]. Na_2CO_3 also plays the role of the template, therefore, the generated macropores further increase the disorder degree of the carbon foam. The appearance of the broad 2D band elucidates that the obtained materials are with great graphitization, which may have a positive effect on maintaining the integrity of the testing structure and efficiently enhance the conductivity of the materials [22].

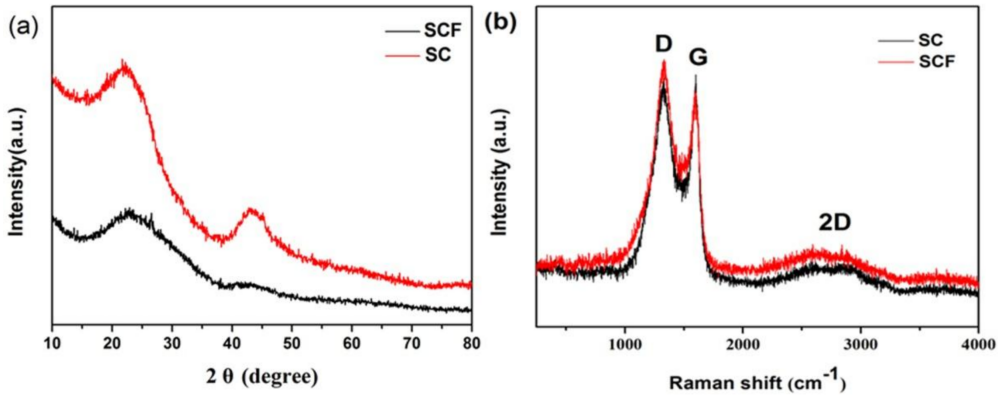

Figure 4. (**a**) X-ray diffraction XRD patterns; (**b**) Raman spectra of SCF and starch-derived carbon SC.

Electrochemical performances of as-obtained materials in 5 M H_2SO_4 are exhibited in Figure 5. The cyclic voltammograms (CVs) of SCF with different scanning rates in Figure 5a show almost rectangular shapes at a potential window ranging from 0 V to −0.8 V referred to as *MSE*. The CV curves of SC and SCF at 10 mVs^{-1} are shown in Figure S2a where SC hardly shows a rectangular shape. The significantly improved current and the quasi-rectangular shapes suggest that more energy can be reserved in the SCF electrode through a fast ion adsorption mechanism [23]. Figure S3 shows CV curves of SC at different scanning rates. In Figure 5b, SCF exhibits a 90.8% capacitance retention with the increasing scan rate from 10 mVs^{-1} to 50 mVs^{-1}, higher than SC. Figure 5c shows the galvanostatic charge-discharge (GCD) curves of SCF at various current densities. Different from the GCD shape of starch-derived carbon (Figure S2b), these profiles are basically linear and symmetric, suggesting the high coulombic efficiency and great reversibility of this material [24]. The specific capacitances of carbon foam calculated from the GCD profiles are 179.6, 168.7, 164, 135, and 113 $F{\cdot}g^{-1}$ at 0.5, 1, 2, 5, and 10 $A{\cdot}g^{-1}$, respectively. With the increasing current densities from 0.5 $A{\cdot}g^{-1}$ to 10 $A{\cdot}g^{-1}$, SCF exhibits a 61.8% capacitance retention in Figure 5d, higher than SC electrode. To further investigate the cycling stability of carbon foam, galvanostatic charge/discharge tests for 1000 cycles at a current density of 0.5 $A{\cdot}g^{-1}$ was conducted. After 1000 cycles, there was 98.9% capacitance retention at 0.5 $A{\cdot}g^{-1}$ (Figure 5e). Figure 5f shows the Nyquist plots of SCF and SC electrodes in the frequency range of0.01 Hz–100 kHz. The value of the EIS curve intersection at the Z′ axis shows the internal resistance (R_s). The smaller diameter of the semicircle in the high-frequency region manifests the smaller charge transfer resistance (R_{ct} = 0.243 Ω), which relates to the conductivity and porous texture of SCF [19,25]. In the set of Figure 5f, the shorter length of the Warburg impedance (W) area with a 45-degree slope reveals the lower ion transportation resistance and better ion diffusion, which results in the great rate capability of SCF [26]. In the low-frequency region, SCF exhibits a steep line with a higher slope, indicating better capacitive performance [27].

The supercapacitive property comparison of SCF and other previously reported carbonaceous materials are summarized in Table 1. The great capacitive performance mainly benefits from its highly developed micropores that guarantee a large surface area for charge accommodation. The excellent rate and cycle capabilities of SCF can be attributed to the massive macropores and mesopores. The former acts as ion-buffering reservoirs to minimize the ion diffusion distances and the latter provides low resistant pathways for ion transportation [28].

Table 1. Comparison of previously reported carbonaceous materials for supercapacitors.

Precursor	S_{BET} (m^2g^{-1})	Capacitance (Fg^{-1})	Current Density (Ag^{-1})	Electrolyte	References
banana peel	1650	206	1	6 M KOH	[29]
luffa sponge	1510	167	1	1 M Na_2SO_4	[30]
animal bone	2157	185	0.05	7 M KOH	[31]
lignite	3162	295	0.04	6 M KOH	[19]
olive residues	1626	193	0.25	1 M H_2SO_4	[32]
waste coffee beans	1019	368	0.05	1 M H_2SO_4	[33]
starch	1157	144	0.05	6 M KOH	[34]
starch	1167	162	0.625	6 M KOH	[35]
starch	1693	179	0.5	5 M H_2SO_4	This work

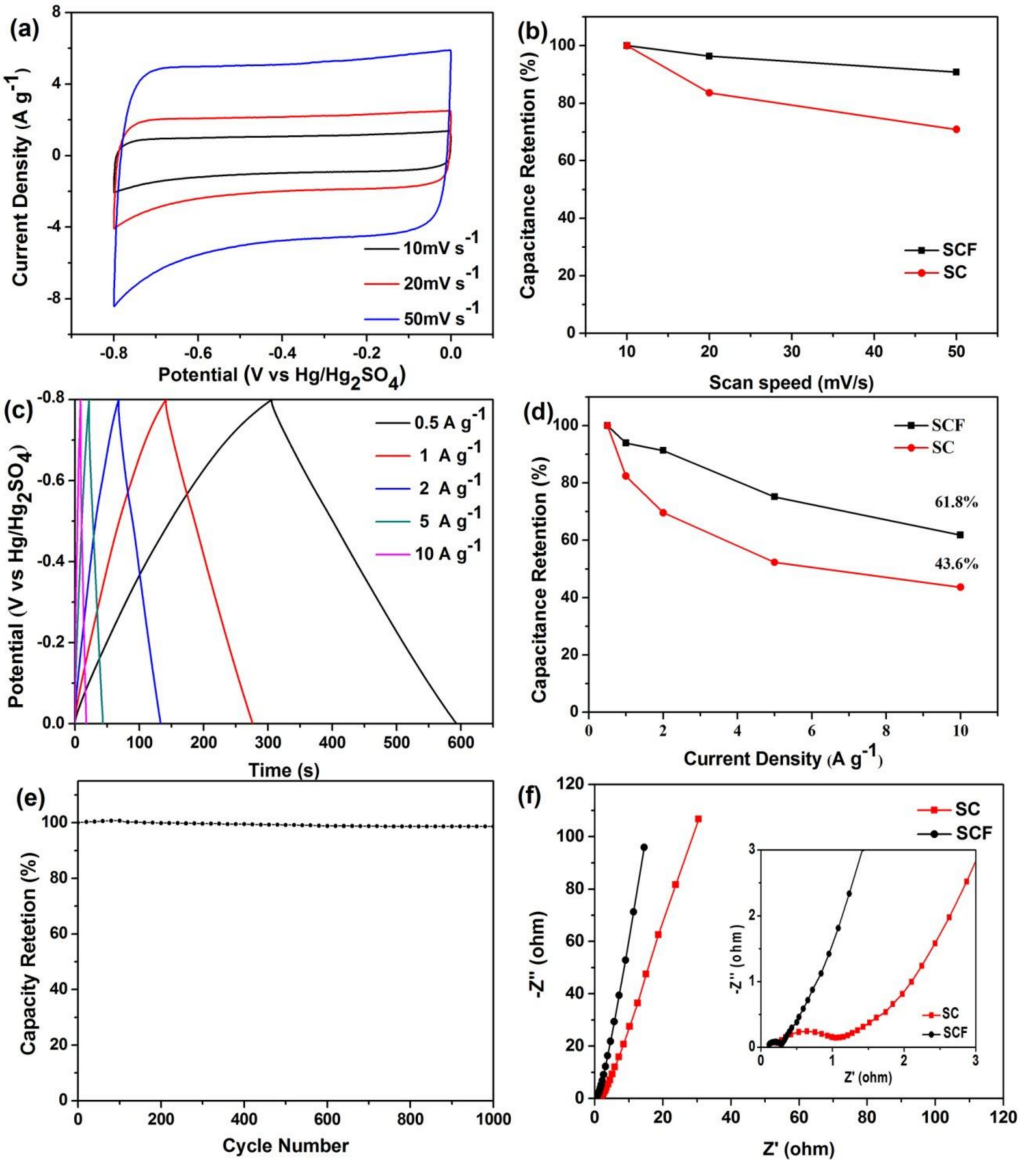

Figure 5. Electrochemical performances are measured in a three-electrodesystem using 5 M H_2SO_4 astheelectrolyte. (**a**) Cyclic voltammogram CV curves of SCF at different scanning rates; (**b**) Capacitance retentions of SCF and SC at different scanning speeds; (**c**) Galvanostatic charge-discharge GCD curves of SCF at different current densities; (**d**) Capacitance retentions of SCF and SC at different currents densities; (**e**) Cycling stability of SCF at 0.5 $A \cdot g^{-1}$; (**f**) Nyquist plots of SCF and SC electrodes in the frequency range of 0.01 Hz–100 kHz with the inset showing the high and middle frequency region.

4. Conclusions

In summary, we present a facile and scalable approach to obtain a well-interconnected 3D carbon foam whose pores are properly distributed by adding Na_2CO_3. The investigations on structure show that Na_2CO_3 plays the roles of the template for the creation of macropores and the activator used to produce the micropores and mesopores. The SCF exhibits a large specific surface area, high conductivity, and hierarchically porous characteristics, which could not only promote the formation of the electric double layer but also ensure the rapid mass transport channel during the charge/discharge process. Therefore, we think that the as-prepared sample is a prospective candidate for the energy storage application.

Supplementary Materials: The following are available online at http://www.mdpi.com/2076-3417/8/4/565/s1, Figure S1: N_2 adsorption/desorption isotherm of SC and the corresponding pore size distribution in the inset. Figure S2: (a) CV curves of SC and SCF at 10 mVs^{-1}; (b) GCD curves of SC and SCF at 0.5 Ag^{-1}. Figure S3: CV curves of SC at different scanning rates in 5M H2SO4.

Acknowledgments: This work is supported by The National Key Research and Development Plan of China (2016YFC0305004).

Author Contributions: Yunfang Gao conceived and designed the experiments; Liangpo Cai performed the experiments; Xin Xu analyzed the data; Jie Ying contributed reagents/materials/analysis tools; Liangpo Cai wrote the paper.

Conflicts of Interest: The authors declare no conflict of interest.

References

1. Zhu, J.; Xu, D.; Wang, C.; Qian, W.; Guo, J.; Yan, F. Ferric citrate-derived n-doped hierarchical porous carbons for oxygen reduction reaction and electrochemical supercapacitors. *Carbon* **2017**, *115*, 1–10. [CrossRef]
2. Jing, T.; Jian, L.; Torad, N.L.; Kimura, T.; Yamauchi, Y. Tailored design of functional nanoporous carbon materials toward fuel cell applications. *Nano Today* **2014**, *9*, 305–323.
3. Chen, Y.; Wen, C.; Wang, C.; Ho, C.; Lin, S.; Chen, Y. Characterization of Transition-Metal Oxide Deposition on Carbon Electrodes of a Supercapacitor. *Appl. Sci.* **2016**, *6*, 413. [CrossRef]
4. Yi, W. Activated Carbon Microtubes Prepared from Plant Biomass (Poplar Catkins) and Their Application for Supercapacitors. *Chem. Lett.* **2014**, *43*, 216–218.
5. Yang, J.; Weng, W.; Zhang, Y.; Du, X.; Liang, Y.; Yang, L. Highly flexible and shape-persistent graphenemicrotube and its energy storage performance. *Carbon* **2018**, *126*, 419–423. [CrossRef]
6. Yu, M.; Zhang, L.; He, X.; Yu, H.; Han, J.; Wu, M. 3D interconnected porous carbons from MOF-5 for supercapacitors. *Mater. Lett.* **2016**, *172*, 81–84. [CrossRef]
7. Wu, X.; Jiang, L.; Long, C.; Fan, Z. From flour to honeycomb-like carbon foam: Carbon makes room for high energy density supercapacitors. *Nano Energy* **2015**, *13*, 527–536. [CrossRef]
8. Zhang, M.; Jia, Y.; Li, H.; Wang, J. A facile method to synthesise reduced graphene oxide/carbon nanotube hybrid fibers as binder-free electrodes for supercapacitors. *Synth. Met.* **2017**, *232*, 66–71. [CrossRef]
9. Lu, H.; Li, Q.; Guo, J.; Song, A.; Gong, C.; Zhang, J. Hierarchically porous carbon with high-speed ion transport channels for high performance supercapacitors. *Appl. Surf. Sci.* **2018**, *427*, 992–999. [CrossRef]
10. Li, M.; Liu, C.; Cao, H.; Zhao, H.; Fan, Z. KOH self-templating synthesis of three dimensional hierarchical porous carbon materials for high performance supercapacitors. *J. Mater. Chem. A* **2014**, *2*, 14844–14851. [CrossRef]
11. Chen, C.; Yu, D.; Zhao, G.; Du, B.; Tang, W.; Sun, L.; Flemming, B.; Yu, M. Three-dimensional scaffolding framework of porous carbon nanosheets derived from plant wastes for high-performance supercapacitors. *Nano Energy* **2016**, *27*, 377–389. [CrossRef]
12. Zhao, C.; Wang, W.; Yu, Z.; Zhang, H.; Wang, A.; Yang, Y. Nano-$CaCO_3$ as template for preparation of disordered large mesoporous carbon with hierarchical porosities. *J. Mater. Chem.* **2010**, *20*, 976–980. [CrossRef]
13. Xie, Q.; Bao, R.; Xie, C.; Zheng, A.; Wu, S.; Zhang, Y. Core-shell n-doped active carbon fiber@graphene composites for aqueous symmetric supercapacitors with high-energy and high-power density. *J. Power Sources* **2016**, *317*, 133–142. [CrossRef]
14. Wang, H.; Zhong, Y.; Li, Q.; Yang, J.; Dai, Q. Cationic starch as a precursor to prepare porous activated carbon for application in supercapacitor electrodes. *J. Phys. Chem. Solids* **2008**, *69*, 2420–2425. [CrossRef]
15. Zhang, J.; Zhang, W. Facile preparation of water soluble phenol formaldehyde resin-derived activated carbon by Na_2CO_3 activation for high performance supercapacitors. *Mater. Lett.* **2017**, *206*, 67–70. [CrossRef]
16. Lu, W.; Huang, S.; Miao, L.; Liu, M.; Zhu, D.; Li, L.; Duan, H.; Xu, Z.; Gan, L. Synthesis of MnO_2/N-doped ultramicroporous carbon nanospheres for high-performance supercapacitor electrodes. *Chin. Chem. Lett.* **2017**, *28*, 1324–1329. [CrossRef]
17. Pang, J.; Zhang, W.; Zhang, J.; Cao, G.; Han, M.; Yang, Y. Facile and sustainable synthesis of sodium lignosulfonate derived hierarchical porous carbons for supercapacitors with high volumetric energy density. *Green Chem.* **2017**, *19*, 3916–3926. [CrossRef]

18. Jiang, H.; Lee, P.S.; Li, C. 3D carbon based nanostructures for advanced supercapacitors. *Energy Environ. Sci.* **2013**, *6*, 41–53. [CrossRef]
19. Wu, Y.; Cao, J.; Zhao, X.; Hao, Z.; Zhuang, Q.; Zhu, J.; Wang, X.; Wei, X. Preparation of porous carbons by hydrothermal carbonization and KOH activation of lignite and their performance for electric double layer capacitor. *Electrochim. Acta* **2017**, *252*, 397–407. [CrossRef]
20. Zou, B.; Zhang, Y.; Wang, J.; Liang, X.; Ma, X.; Chen, C. Hydrothermally enhanced MnO/reduced graphite oxide composite anode materials for high performance lithium-ion batteries. *Electrochim. Acta* **2015**, *167*, 25–31. [CrossRef]
21. Zhang, H.; Zhang, G.; Li, Z.; Qu, K.; Wang, L.; Zeng, W. Ultra-uniform Cuo/Cu in nitrogen-doped carbon nanofibers as a stable anode for li-ion batteries. *J. Mater. Chem. A* **2016**, *4*, 10585–10592. [CrossRef]
22. Chen, Z.; Wang, T.; Zhang, M.; Cao, G. Energy storage: A phase-separation route to synthesize porous CNTs with excellent stability for Na+ storage. *Small* **2017**, *13*, 1604045. [CrossRef] [PubMed]
23. Cheng, P.; Gao, S.; Zang, P.; Yang, X.; Bai, Y.; Xu, H.; Liu, Z.; Lei, Z. Hierarchically porous carbon by activation of shiitake mushroom for capacitive energy storage. *Carbon* **2015**, *93*, 315–324. [CrossRef]
24. Zhang, D.; Zhao, J.; Feng, C.; Zhao, R.; Sun, Y.; Guan, T. Scalable synthesis of hierarchical macropore-rich activated carbon microspheres assembled by carbon nanoparticles for high rate performance supercapacitors. *J. Power Sources* **2017**, *342*, 363–370. [CrossRef]
25. Tian, Y.; Li, D.; Liu, J.; Wang, H.; Zhang, J.; Zheng, Y. Facile synthesis of Mn_3O_4 nanoplates-anchored graphene microspheres and their applications for supercapacitors. *Electrochim. Acta* **2017**, *257*, 155–164. [CrossRef]
26. Liu, J.; Li, H.; Zhang, H.; Liu, Q.; Li, R.; Li, B. Three-dimensional hierarchical and interconnected honeycomb-like porous carbon derived from pomelo peel for high performance supercapacitors. *J. Solid State Chem.* **2018**, *257*, 64–71. [CrossRef]
27. Yang, X.; Du, G.; Zhang, L.; Liu, Y. Preparation of hierarchical porous carbon material derived from starch for high-performance electrochemical capacitor. *Mater. Lett.* **2016**, *183*, 52–55. [CrossRef]
28. Chen, Y.; Gao, Z.; Zhang, B.; Zhao, S.; Qin, Y. Graphene coated with controllable n-doped carbon layer by molecular layer deposition as electrode materials for supercapacitors. *J. Power Sources* **2016**, *315*, 254–260. [CrossRef]
29. Lv, Y.; Gan, L.; Liu, M.; Xiong, W.; Xu, Z.; Zhu, D. A self-template synthesis of hierarchical porous carbon foams based on banana peel for supercapacitor electrodes. *J. Power Sources* **2012**, *209*, 152–157. [CrossRef]
30. Li, J.; Ren, Z.; Ren, Y.; Zhao, L.; Wang, S.; Yu, J. Activated carbon with micrometer-scale channels prepared from luffa sponge fibers and their application for supercapacitors. *RSC Adv.* **2014**, *4*, 35789–35796. [CrossRef]
31. Huang, W.; Zhang, H.; Huang, Y.; Wang, W.; Wei, S. Hierarchical porous carbon obtained from animal bone and evaluation in electric double-layer capacitors. *Carbon* **2011**, *49*, 838–843. [CrossRef]
32. Elmouwahidi, A.; Bailón-García, E.; Pérez-Cadenas, A.F.; Maldonado-Hódar, F.J.; Carrasco-Marín, F. Activated carbons from koh and H_3PO_4 -activation of olive residues and its application as supercapacitor electrodes. *Electrochim. Acta* **2017**, *229*, 219–228. [CrossRef]
33. Rufford, T.; Hulicova-Jurcakova, D.; Zhu, Z.; Lu, G.Q. Nanoporous carbon electrode from waste coffee beans for high performance supercapacitors. *Electrochem. Commun.* **2008**, *10*, 1594–1597. [CrossRef]
34. Wu, M.; Ai, P.; Tan, M.; Jiang, B.; Li, Y.; Zheng, J. Synthesis of starch-derived mesoporous carbon for electric double layer capacitor. *Chem. Eng. J.* **2014**, *245*, 166–172. [CrossRef]
35. Pang, L.; Zou, B.; Han, X.; Cao, L.; Wang, W.; Guo, Y. One-step synthesis of high-performance porous carbon from corn starch for supercapacitor. *Mater. Lett.* **2016**, *184*, 88–91. [CrossRef]